JCARME
ISSN: 2228-7922
Journal of Computational and Applied Research in Mechanical Engineering
Vol. 4, No. 1, pp. 1- 17, Autumn 2014
http://jcarme.srttu.edu

Fracture mechanics-based life prediction of a riveted lap joint

A. R. Shahani* and H. Moayeri Kashani

Fracture Mechanics Research Laboratory, Department of Applied Mechanics, Faculty of Mechanical Engineering, K.N. Toosi University of Technology, P.O Box 19395-1999, Tehran, Iran

Article info:
Received: 15/05/2013
Accepted: 15/03/2014
Online: 11/09/2014

Keywords:
Riveted Lap Joints,
Fatigue Crack Growth Profiles,
EIFS,
Life Prediction.

Abstract
In this paper, three-dimensional modeling of the fatigue crack growth profiles was performed in a simple riveted lap joint. Simulation results showed that mode I was dominated on the one side of the plates and the crack straightly grew on this side, while the other side of the plates was in a mixed-mode condition and the crack propagation path was not straight on this side. Afterward, the fracture mechanics-based life prediction of the riveted lap joint was considered using EIFS concept. Back extrapolation method was used for estimating EIFS. Results demonstrated that EIFS would depend on loading amplitude if ΔK had been implemented in EIFS estimation using Paris equation. In contrast EIFS dependency on loading amplitude significantly reduced when using ΔJ in EIFS estimation. Finally, fatigue life of the riveted lap joint was predicted based on safe life method using Brown-Miller critical plane criterion. Results represented that the predicted life using fracture mechanics concept was much closer to the experimental results.

Nomenclature

a	Crack length (m)	$g_L(a)$	Large crack growth curve
a_i	Initial crack length (m)	$g_S(a)$	Small crack growth curve
a_f	Final crack length (m)	IFS	Actual initial flaw size
A	Constant exponent in the equation	J	J-integral (MPa.m)
b	Fatigue strength exponent	K	Stress intensity factor (MPa.√m)
B	Constant exponent in the equation	m	Constant exponent in the equation
c	Fatigue ductility exponent	m'	Constant exponent in the equation
C'	Constant exponent in the equation	n	Constant exponent in the equation
C^*	Constant exponent in the equation	N	Number of cycles
$\bar{C}$	Constant exponent in the equation	N_f	Life
da/dN	Fatigue crack growth rate (m/cycle)	R	Stress ratio
E	Material elastic modulus (MPa)	S	Constant coefficient in the equation
$EIFS$	Equivalent initial flaw size (mm)	γ_{max}	Maximum shear strain (MPa)
G	Energy release rate (MPa.m)	ε_f'	Fatigue ductility coefficient

*Corresponding author
Email address: shahani@kntu.ac.ir

ε_{max}	Maximum normal strain
σ_f'	Fatigue strength coefficient (MPa)
$\sigma_{n,mean}$	Mean stress on plane of γ_{max}(MPa)
ϑ	Poisson's ratio

1. Introduction

Rivets are highly used in aircraft fuselage manufacturing and repairing processes. A large number of rivets are used for assembling aircraft bodies. For instance, approximately 100,000 solid rivets are utilized for one subassembly of Boeing 747 aircraft [1]. Therefore, the integrity of fuselage structures is directly related to the integrity of riveted joints.

Due to the service fatigue loading of the joints in aircraft structures, fatigue types of failure are the most common failure types in an aircraft fuselage. There are various criteria for fatigue life prediction of structures; some of the available methods are depicted in Fig. 1.

In this figure, fatigue life prediction methods are divided into two general safe-life and damage tolerance design concepts. The first group is a conventional method which is itself divided into three stress-based, strain-based, and energy-based approaches [2]. The second group is fracture mechanics approach which is based on fatigue crack growth.

The existing variety of concepts in fatigue life prediction has confused designers and engineers in the industry. This question has always been asked that "Which criteria and which methods are more reliable and suitable in designing a structure with determined geometry and loading?" The crack growth theory can form a bridge which connects the concepts of safe-life and fracture mechanics. Merging of these two concepts provides a unified concept for life prediction in the industry [3]. Therefore, fracture mechanics-based life prediction is an applicable and advantageous method in the industry, especially in aerospace industries. It has been a research topic for many international organizations such as AGARD, ASTM, NASA, and CAE since 1992.

In the fracture mechanics-based life prediction method, it is always assumed that an initial crack (similar to the crack which is formed and initiated from voids) exists in the specimen. In fact, this assumption is not far away from the reality for many industrial components or notched specimens in which defects are generated during manufacturing processes. The number of cycles is determined according to the available relations in fatigue crack growth such as Paris Model (Eq. (1)).

$$\frac{da}{dN} = \bar{C}(\Delta K)^m \rightarrow N_f = \int_{a_i}^{a_f} \frac{da}{\bar{C}(\Delta K)^m} \qquad (1)$$

In this relation, the upper limit of the integral can be calculated using the fracture toughness of the material. However, calculation of the initial crack length (a_i) is one of the problems of this method. The initial crack length can be measured by non-destructive tests (NDT). However, the initial flaw size (*IFS*) can be below the current detection capability of the NDT technique. If the NDT detection limit is chosen as the initial flaw size, it will result in a very conservative design [4]. In addition, the behavior of a small crack growth is complicated and dependent on the microstructures of the material. The crack growth behaviors of small and large crack growth rate curves are compared in Fig. 2.

Behavior of a small crack can be profoundly affected by the microstructure. For example, while the crack is within a single crystal grain in a metal, the growth rate is much higher than the expected rate from the usual da/dN versus ΔK curve, as illustrated in Fig. 2. Upon encountering a grain boundary, the growth is temporarily retarded. Until the crack becomes several times larger than the grain size, the average growth rate, as affected by lattice planes within grains and grain boundaries, is considerably above the usual da/dN versus ΔK curve [1].

Thus, two cases can be considered in life prediction based on fracture mechanics concept. In the first case, the lower limit of the integral is

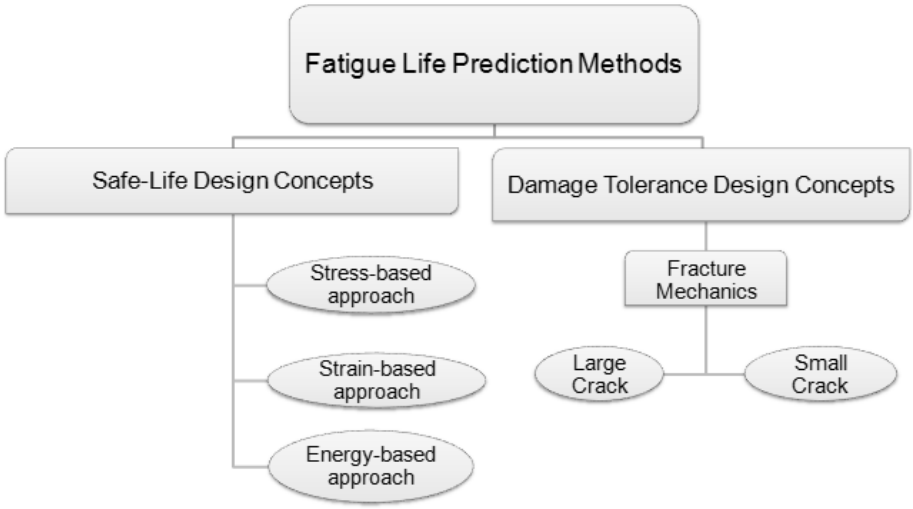

Fig. 1. Available methods in fatigue life estimation**.**

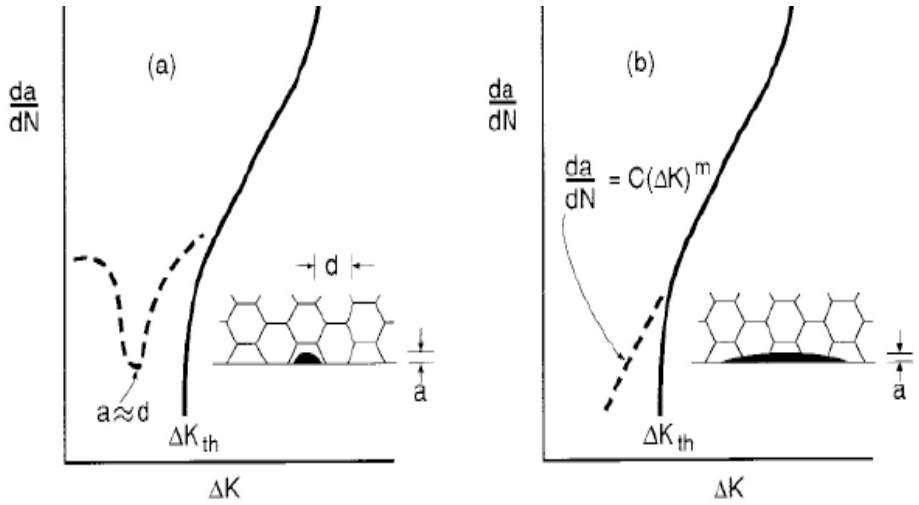

Fig. 2. Comparison between (a) small and (b) large crack growth rate curves.

assumed to be the actual initial flaw size (*IFS*), and the small crack growth curve $g_s(a)$ should be used according to Eq. (2).

$$N_{IFS} = \int_{IFS}^{a_c} \frac{1}{g_s(a)} da \qquad (2)$$

In the second case, the usual large crack growth curve $g_L(a)$ is used instead of the complicated small crack growth curve. In this case, the lower limit of the integral must be replaced with an equivalent initial flaw size (*EIFS*), as presented in Eq. (3).

$$N_{EIFS} = \int_{EIFS}^{a_c} \frac{1}{g_L(a)} da \qquad (3)$$

As demonstrated in Fig. 3, both cases can give the same life prediction if *EIFS* is properly chosen and the underlying areas below $g_s(a)$ and $g_L(a)$ are equal [4].

In order to estimate the *EIFS* value, the underlying areas below $g_s(a)$ and $g_L(a)$ must be equal, as shown in Fig. 3. On the other hand, the *EIFS* concept, which avoids small crack growth analysis, uses an equivalent initial flaw size in large crack growth analysis and estimates the fatigue life to match the experimental one [4]. In other words, instead of matching life predictions obtained from long crack growth and small crack growth analyses, *EIFS* is calculated by matching the life predicted by long crack growth analysis with the one observed in fatigue S-N testing [4].

Newman [5] predicted the life of various notched specimens based on the small crack growth curve with the aid of Fastran software [6]. Main problem of this method is the complexity of small crack theory.

However, life prediction based on *EIFS* concept is an applicable method, which has been considered by numerous researchers [7-9].

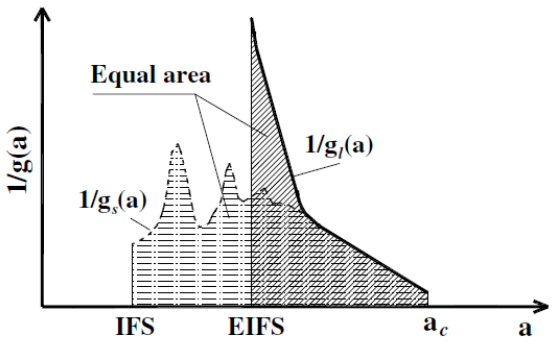

Fig. 3. Equivalent Initial Flaw Size Concepts [4].

Riveted lap joints are susceptible to cracks due to fatigue and fretting [1]. Multiple site damage (MSD) (sometimes called widespread fatigue damage (WFD)) is an important problem associated with aging aircraft, which was started to be studied by Aloha accident in 1988 [10]. MSD is due to fatigue and affects the service life of an aircraft. In MSD type failure, small fatigue cracks grow at different sites in the same structural elements and finally link-up forming large and more dangerous cracks. The crack growth rate is much faster for the case of MSD than the case of an individual crack [11].

Lucas et al. [12] conducted experimental fatigue testing and damage characterization of riveted lap joint and concluded the loading of the lap joint results in a complex 3D stress distribution at the rivet holes resulting from residual stresses, remote loading, and bending stress due to joint eccentricity. They noted that fatigue crack initiation occurred in the regions of high stress concentration at or near rivet holes.

Experimental studies conducted by Piascik et al. [13] showed that fatigue crack initiation occurred in the region of high stress concentration factors located at or near the rivet holes. They found cracks to initiate at the corners of rivet hole, dents, and fretted surfaces.

Moreira et al. [14] carried out three-dimensional FEA to analyze cracked riveted lap joints with three rivet rows and one rivet column. The stress intensity factor determination of the cracks at the rivet hole was also considered. The riveted joint was modeled with no interference (perfect fit joint) and it was

concluded that mode I of fracture was dominant over modes II and III. They did not model the fatigue crack growth profiles.
Skorupa et al. [15] conducted fatigue tests on the specimens from an aircraft Al alloy D16Cz Alclad sheets and concluded that fatigue cracks in riveted lap joints always started in one of the end rivet rows on the faying surface of the loaded sheet.
Park and Atluri [16] and Beuth and Hutchinson [17] have investigated multiple-site cracking in fuselage lap joints.
Harris et al. [18] carried out crack growth analysis of a riveted joint due to fatigue loading using the results of fractographic examination of a rivet hole.
In this paper, 3D simulation of the fatigue crack growth process was performed in a simple riveted lap joint and the crack growth profiles were predicted. Then, the fracture mechanics-based life prediction of the riveted lap joint was considered using EIFS concept. Back extrapolation method was used for estimating EIFS by the aid of both cyclic stress intensity factor (ΔK) and cyclic J integral (ΔJ). Then, the results were compared.
Finally, fatigue life of the riveted lap joint was predicted based on conventional method using Brown-Miller critical plane criterion. The results were compared with the ones obtained from fracture mechanics concept.

2. Numerical modeling of fatigue crack growth profiles

2.1. Procedure

Fatigue crack growth under combined loading can be described in terms of energy release rate, similar to Paris Model, according to Eq. (4) [19].

$$\frac{da}{dN} = C^*(\Delta\sqrt{G})^n \quad (4)$$

where C^* and n are material properties and G is calculated using Eq. (5).

$$G = \frac{B}{E}(K_I^2 + K_{II}^2) + \left(\frac{1+\vartheta}{E}\right)K_{III}^2 \quad (5)$$

in which B is equal to one ($B= 1$) in plane stress conditions, while $B = 1 - \vartheta^2$ holds under plane strain conditions.
Crack propagation direction and the amount of the growth are two essential parameters to be determined in general crack growth analysis. It is complicated to determine the fatigue crack growth direction in the 3D case for an arbitrary crack shape and under combined loading conditions, which is due to the fact that the direction of the crack growth is governed by a combination of all three loading modes KI, KII, and KIII. An appropriate solution is to consider the crack growth direction to be equivalent to the direction of maximum energy release rate [19].
This method is based on virtual crack extension method proposed by Hellen [20] and Billardo [21].
The procedure of the iterative 3D fatigue crack growth prediction method is schematically shown in Fig. 4.
Crack growth starts with an initial size and shape of crack front. Then, the energy release rate is calculated in every node on the crack front and maximum value of energy release rate and its direction are defined. Afterward, crack growth direction and the amount of growth are determined by virtual crack extension method and the crack front is updated. This procedure will be repeated until the crack size or the number of cycles reaches a certain limit.
Fatigue crack growth simulation of the problem is performed by Zencrack software [22].

2.2. FE modeling

In this section, a simple riveted lap joint with three-row and one-column rivets according to Fig. 5 is modeled using FEM. Geometry and material were the same as those reported by Moreira et al. [14]. The plates and rivets were made of Aluminum 2024-T3 and Aluminum 2117-T4, respectively. Mechanical properties of the plates and the rivets are given in Table 1.
The diameter and length of the rivets were *3.2 (mm)* and *7 (mm)*, respectively.

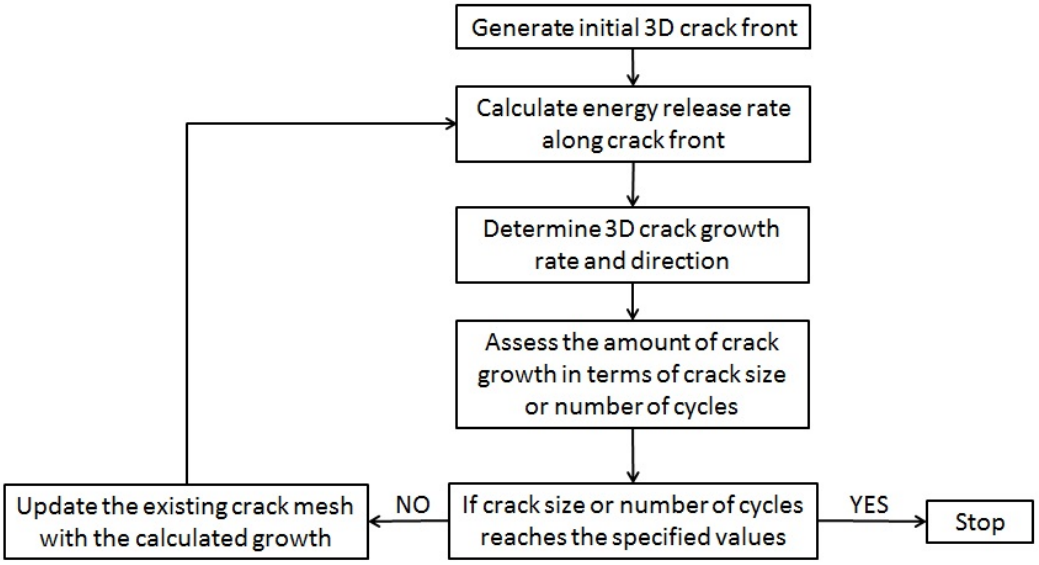

Fig. 4. Iterative procedure of 3D crack growth in ZENCRACK [19].

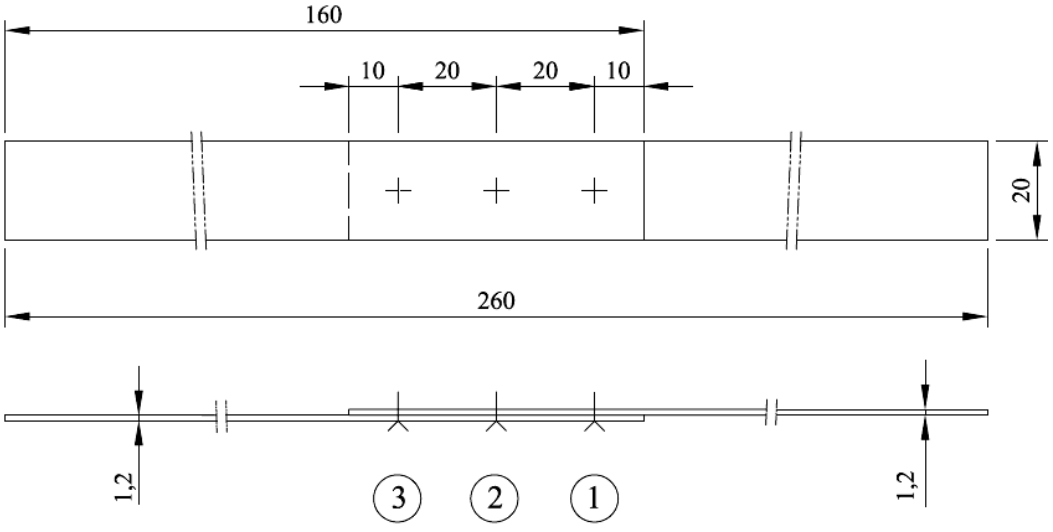

Fig. 5. Lap joint with three rivets [14].

Table 1. Mechanical property of Aluminums 2024-T3 and 2117-T4 [14].

	Aluminium 2024-T3	Aluminium 2117-T4
Density (gr/cc)	2.78	2.75
Elasticity Modulus (GPa)	73.1	71
Poisson Ratio	0.33	0.33
Yield Stress (MPa)	345	165

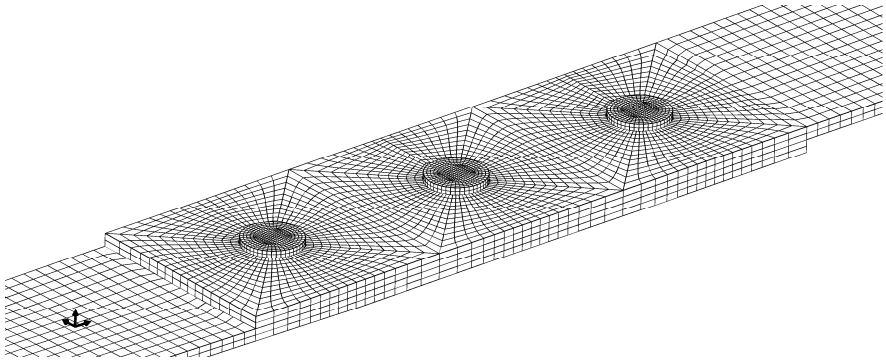

Fig. 6. Finite element model of the problem.

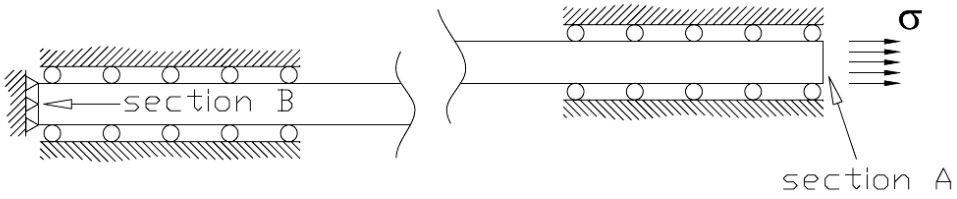

Fig. 7. Applied boundary conditions and loading [14].

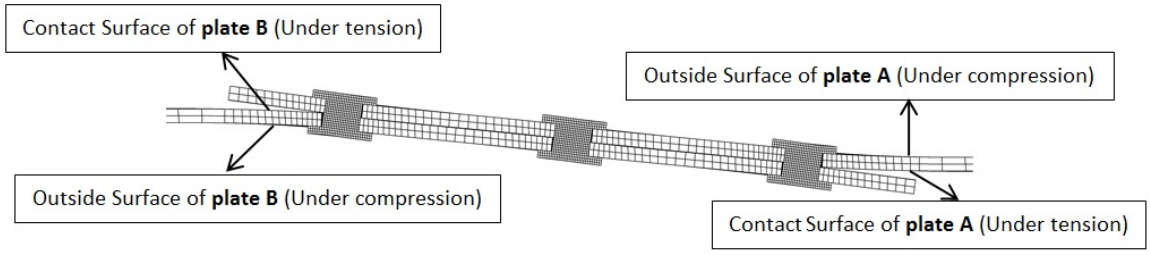

Fig. 8. Bending of plates after applying load.

Three-dimensional simulation of the problem was performed in ABAQUS software. Fig. 6 depicts the meshed model including 22320 second-order quadratic elements (C3D20R).

The remote load was applied to section A of the top plate (Fig. 7). All of the nodes of the section B were constrained in all three degrees of freedom. The applied load was equal to *90, 120, and 160 (MPa)* with the stress ratio of *R=0.05*.

The first and last rivets supported the majority of the load and it was observed in the experimental tests that the cracks occurred in the cross section containing rivet 1 of the upper plate and rivet 3 of the lower one (see Fig. 5) [14].

As shown in Fig. 8, the plates were bended under tensional loading. Thus, combined loading conditions existed around the riveted holes. The outside surface of plate B was under tensile stress and its contact surface was under compressive stress. But, the outside surface of plate A was under compressive stress and its contact surface was under tensile stress.

Two symmetric through cracks were modeled in the first and third rivets of plates A and B (Fig. 9) in order to simulate fatigue crack growth process according to the iterative procedure presented in Fig. 4. This crack geometry was an approximation of the real geometry occurring during the fatigue loading of the specimen since it was expected that, due to secondary bending, cracks would initiate and grow during a part of the fatigue life time as a part through cracks (typically with the quarter of ellipse shape) [14]. The initial crack length was assumed to be a_i*= 1.8 (mm)* (note that *a*(mm) includes hole radius).

Singular elements were used at the crack tip in order to increase the the simulation accuracy according to Fig. 10.

Fig. 12 shows the distribution of stress intensity factor along the thickness of plate B. It can be observed that maximum stress intensity factor appeared at the contact surface of the plate which was under tension due to the applied bending.

As shown in Fig. 13, the crack mouth opening on the contact surface was also greater than the one on the outside surface.

Stress intensity factors in the three modes are compared in Fig. 14.

Fig. 11 shows the predicted fatigue crack growth profiles in the first rivet hole of plate B. As given in this figure, the crack tip on the contact surface, which was under tension stress, grew more than the crack tip on the outside surface which was under compression stress.

It can be seen that, on the contact surface of plate B, the value of the stress intensity factor in the first mode was much greater than the one in other modes. Therefore, mode I was dominated and the crack straightly grew on this surface. But the outside surface of plate B was in the mixed-mode condition. Thus, the crack propagation direction gradually changed on this surface (Fig. 15).

In Fig. 16, the predicted crack propagation direction on the outside surface of plate B was compared with the experimental observation. Fig. 17 shows the predicted fatigue crack growth profiles in the first rivet hole of plate B. As mentioned before, the contact surface was in mode I condition, while the outside surface was in the mixed-mode condition. Thus, the out-of-plane crack growth profiles occurred.

It is necessary to mention that, in the F.E. modeling performed by Moreira et al. [14], it was assumed that the amount and direction of the crack growth were the same on both contact and outside surfaces. In contrast the experimental observations [11] as well as the obtained results from the present study (Figs. 15 and 16) showed that the crack straightly grew on the contact surface; but, the crack propagation direction gradually changed on the outside surface.

Thus, as in Fig. 18, the SIF obtained from the results of the present study was in good agreement with the one obtained from the results of the Moreira's research [14] only on the contact surface.

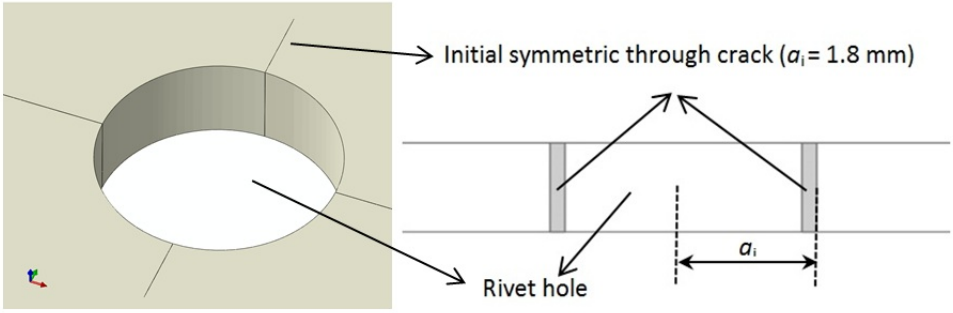

Fig.9. Initial symmetric through crack at the riveted hole.

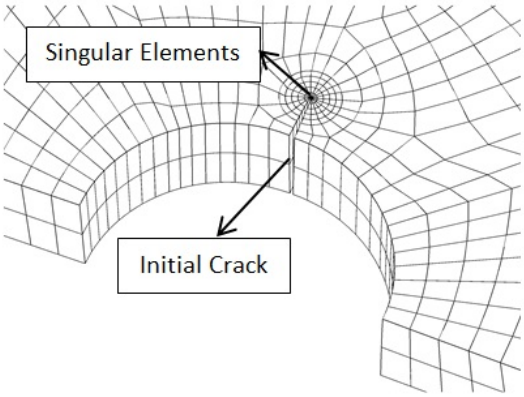

Fig. 10. Singular elements at the crack tip.

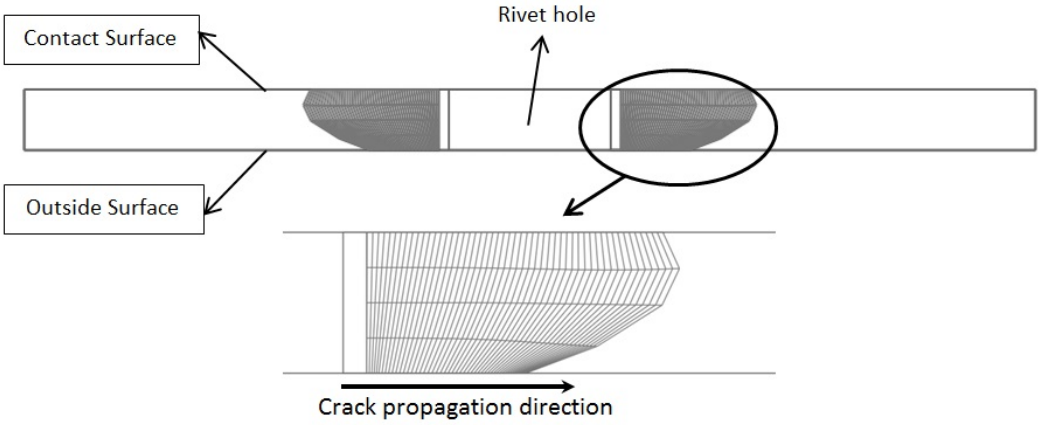

Fig. 11. Predicted fatigue crack growth profiles in the first rivet hole of the plate B.

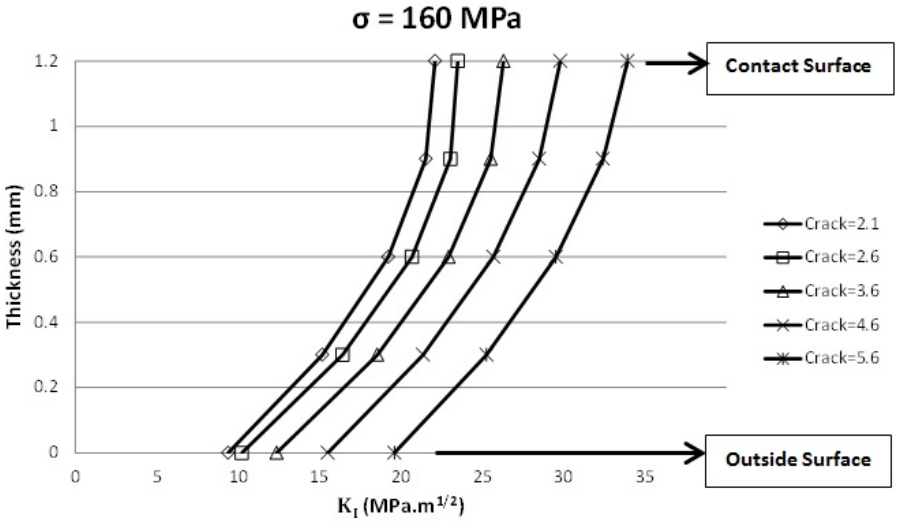

Fig. 12. Distribution of stress intensity factor along the thickness of the plate B in different crack lengths.

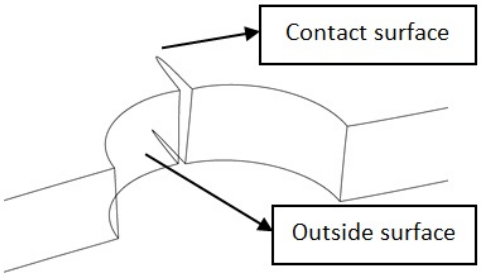

Fig. 13. Non-uniform crack mouth opening displacement across the thickness of plate B.

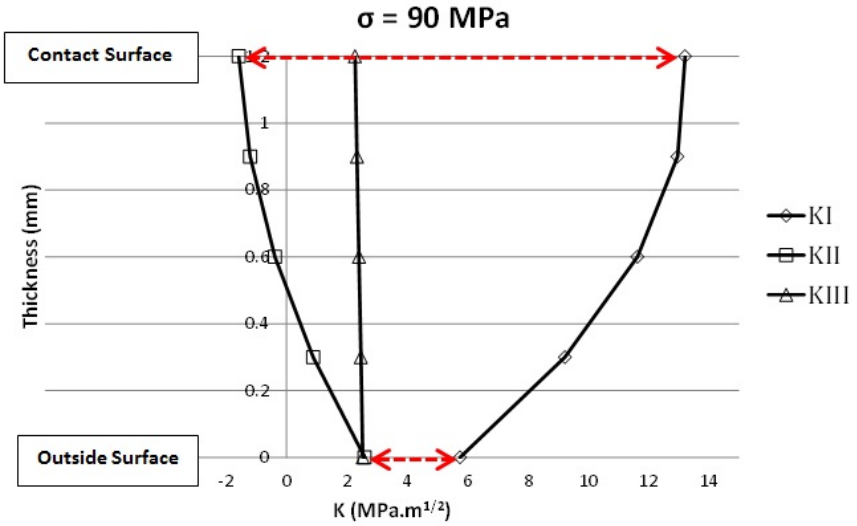

Fig. 14. Comparison of the stress intensity factors in three modes (crack length on the contact surface=2.6 mm).

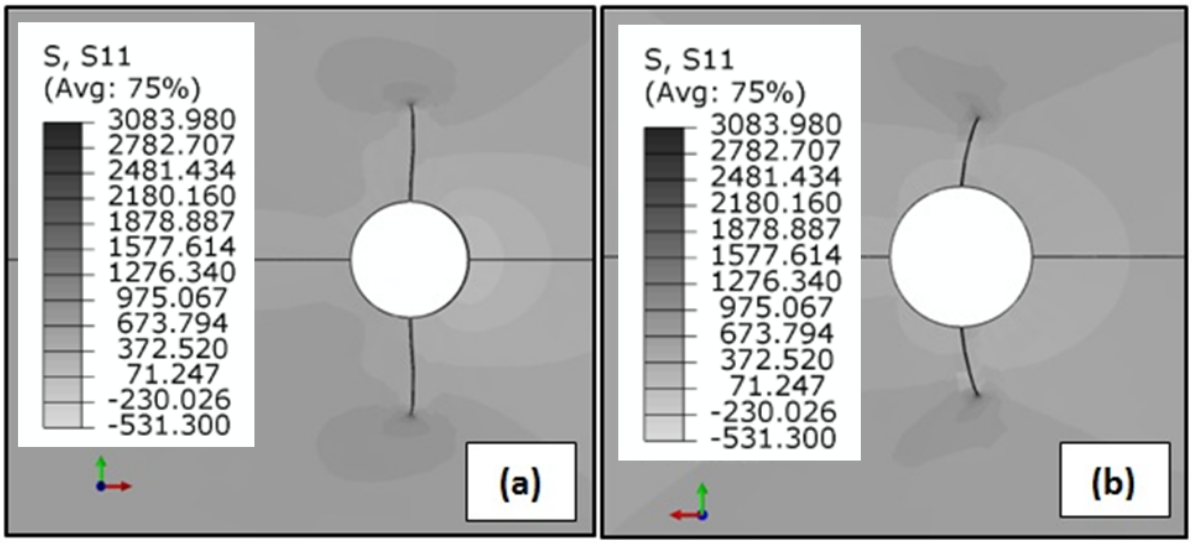

Fig. 15. Crack propagation direction on the (a) contact surface (b) outside surface.

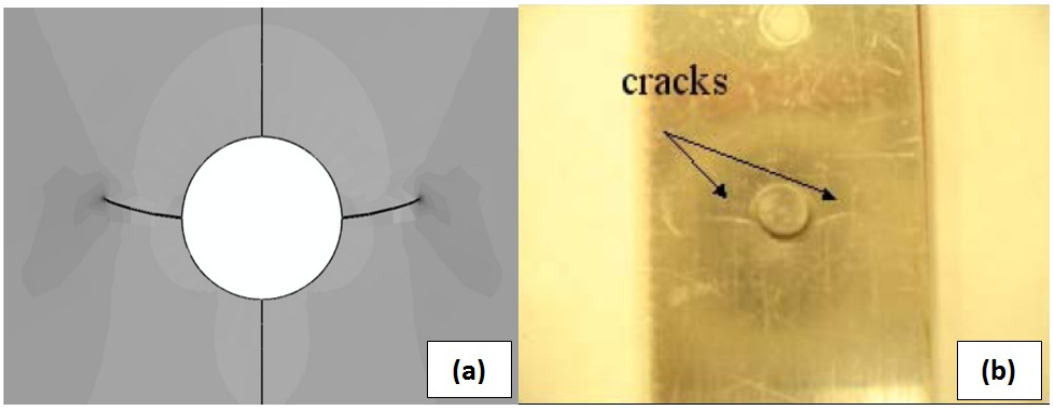

Fig. 16. (a) Predicted crack propagation direction (b) Experimental observation [11].

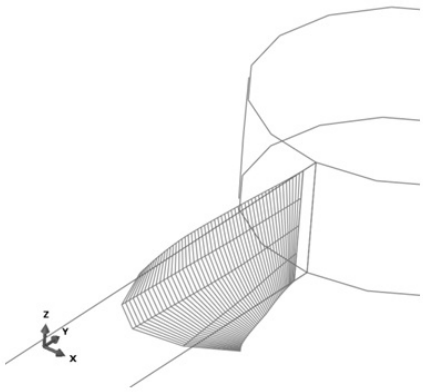

Fig. 17. Out-of-plane crack growth profiles.

3. Estimating equivalent initial flaw size

There are several methods for calculating *EIFS*, the most applicable of which is back extrapolation method. The algorithm of this method is illustrated in Fig. 19.
According to this method, at first, the life is measured by conducting experimental fatigue tests. Assuming a pre-existing crack with the specified initial length, the life of the specimen is predicted using Paris model. Finally, the life of the specimen which is obtained in the laboratory is compared with the predicted one. Afterwards, the assumed initial crack length is modified in the subsequent analyses until an appropriate error is achieved.
One of the main problems in this method is the dependency of *EIFS* on load level, which means that the estimated *EIFS* changes with the variation of load amplitude.
In this paper, *EIFS* was calculated based on both cyclic stress intensity factor and cyclic J-integral in the riveted lap joint.
EIFS dependency on the load level was studied in both cases, which will be discussed later.

3.1. Estimating EIFS using cyclic stress intensity factor

This section considers the calculation of *EIFS* using Paris model. EIFS was estimated based on the values of the stress intensity factor on the contact surface of plate B and mode I was assumed to dominate this surface.
Coefficients of Paris model for AL2024-T3 were also *m=3.3736* and *C=5.0227E-11*, respectively [23].
In [14], the life of the mentioned simple lap joint was reported under various applied loads obtained through the fatigue tests (Table 2).
According to the algorithm of Fig. 19, *EIFS* was estimated in such a way that the predicted number of cycles became equivalent to the fatigue life achieved from the experimental results.
Based on the experimental observations, the final crack length was also equal to *4 (mm)* in the contact surface of plate B [14].

Table 2. Riveted lap joint life under different loadings [14].

Life (Cycles)	Loading Values (Mpa)
706350	90
239830	120
79414	160

The predicted values for *EIFS* are specified in Table 3. It can be observed that the amount of EIFS was not constant and depended on the applied load level.

Table 3. Estimated amounts of EIFS using ΔK.

EIFS (mm)	Loading Values (Mpa)
3.707	90
3.734	120
3.764	160

3.2. Estimating EIFS using cyclic J integral

Some relations other than Paris model have been previously presented for simulating fatigue crack growth. Shahani et al. [24] presented the following relation for fatigue crack growth.

$$\frac{da}{dN} = C'(\Delta J)^{m'} \tag{6}$$

where:

$$m' = \frac{m}{2}$$
$$C' = \bar{C}[E\frac{(1-R)}{(1+R)}]^{\frac{m}{2}} \tag{7}$$

The experimental results conducted by Shahani et al. [24] showed that ΔJ, contrary to ΔK, varied with the variations of R-ratio.
Therefore, there is no need to enter R parameter directly into the well-known Paris equation if ΔJ parameter is used instead of ΔK in this equation.
Unlike those of Paris equation, constants of these equations are independent from loading[24].
Accordingly, Eq. (6) is used to predict the *EIFS* in this section.
The predicted values for *EIFS* based on J integral are given in Table 4.

It can be seen that, in this case, *EIFS* variations due to different load values decreased significantly in such a way that can almost be assumed as a constant.
The simulation results showed that *EIFS* depended on the loading amplitude if cyclic stress intensity factor was implemented in *EIFS* estimation; in contrast, when using *J*-integral in *EIFS* estimation, its dependency on load amplitude reduced significantly in such a way that can be assumed as a constant (Fig. 20).

Table 4. Estimated EIFS values using ΔJ.

EIFS (mm)	Loading Values (Mpa)
3.7688	90
3.7666	120
3.7651	160

4. Life prediction

4.1. Fracture mechanics-based life prediction

In this section, the life of the riveted lap joint is estimated using the average amount of estimated *EIFS* by cyclic *J*-integral method which was considered to be equal to *EIFS=3.7668 (mm)* using Eq. (6).
According to Fig. 21, it can be realized that the predicted life based on fracture mechanics was in very good agreement with the experimental results, as was expected.

4.2. Life prediction using Brown-Miller critical plane criterion

In this section, the life prediction of the lap joint is studied based on B&M criterion. For this purpose, the stress and strain fields were driven by the finite element analysis made on the riveted lap joint without considering cracks.
Drapper [25] mentioned that Brown-Miller critical plane criterion was more accurate for ductile materials than other criteria. Brown and Miller considered a critical plane, in which the shear strain amplitude was maximum [26]. The cyclic shear strains caused crack initiation, whereas cyclic normal strains caused crack propagation [26]. Therefore, they suggested Eq. (8) for the life estimation of structures.

$$\frac{\Delta\gamma_{max}}{2} + S\Delta\epsilon_n = A\frac{\sigma_f'}{E}(2N_f)^b + B\,\epsilon_f'\,(2N_f)^c \quad (8)$$

in which σ_f' and b are material constants obtained from stress-life diagram according to ASTM E466 standard [27]. ϵ_f' and c is also measured in the laboratory from strain-life diagram, as stated by ASTM E606 standard [28]. A and B coefficients are calculated using Eq. (9) and S is also a material constant.

$$\begin{aligned} A &= 1.3 + 0.7S \\ B &= 1.5 + 0.5S \end{aligned} \quad (9)$$

By implementing Morrow mean stress method in this criterion, the effect of mean stress was also reflected according to Eq. (10).

$$\frac{\Delta\gamma_{max}}{2} + \frac{\Delta\epsilon_n}{2} = A\frac{\sigma_f' - 2\sigma_{n,mean}}{E}(2N_f)^b + B\,\epsilon_f'\,(2N_f)^c \quad (10)$$

It has to be noted that the mean stress $\sigma_{n,mean}$ on the maximum shear strain amplitude plane is equal to half of the axial mean stress [26].
The Constants of Eq. (10) for AL2024-T3 are given in Table 5 [29].
Fig. 22 depicts the comparison between the predicted life by B&M critical plane criterion and the one that predicted by fracture mechanics using EIFS concept.
It is observed that the life estimated by B&M criterion has no good accuracy (maximum error is 72.4%) as compared to the fracture mechanics approach.

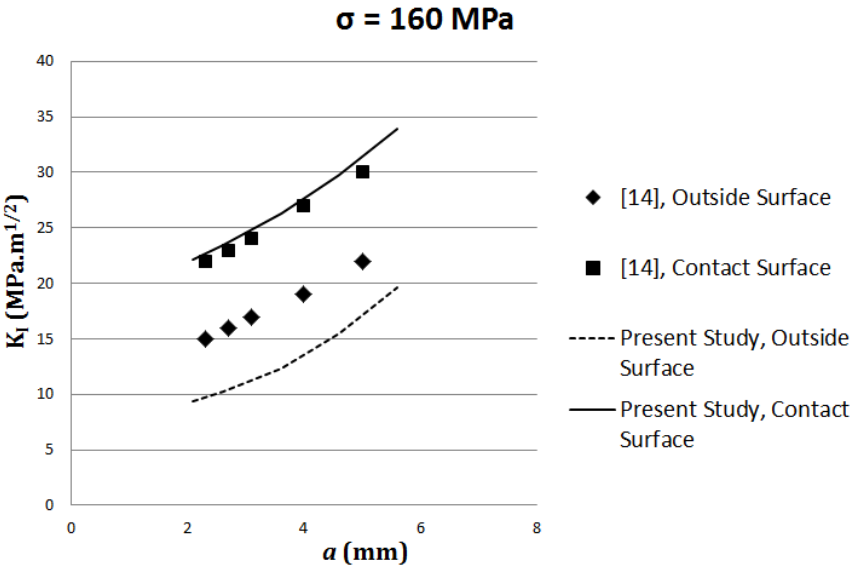

Fig. 18. Comparing the SIF obtained from the results of the present study with the one obtained from the results of the Moreira's research [14].

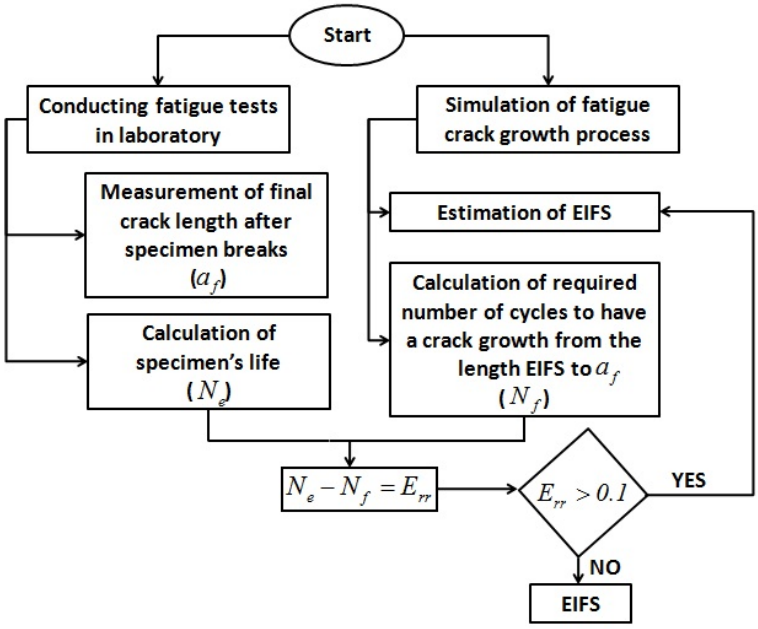

Fig. 19. Algorithm of back-extrapolation method.

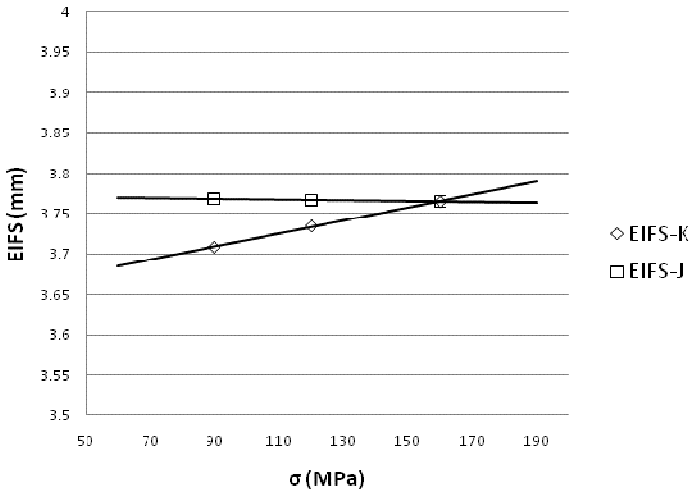

Fig. 20. Comparison of EIFS estimated by stress intensity factor and J integral methods.

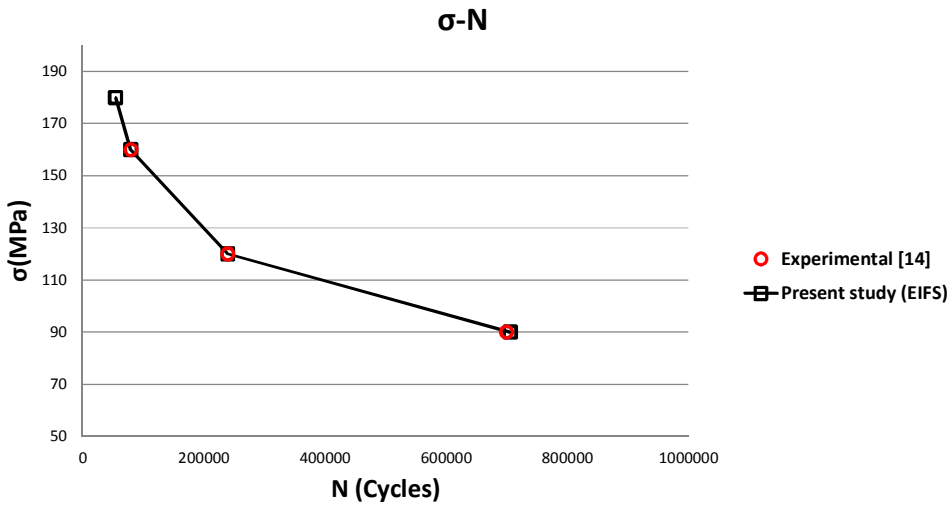

Fig. 21. Comparison of predicted life from fracture mechanics concept with that of experimental results.

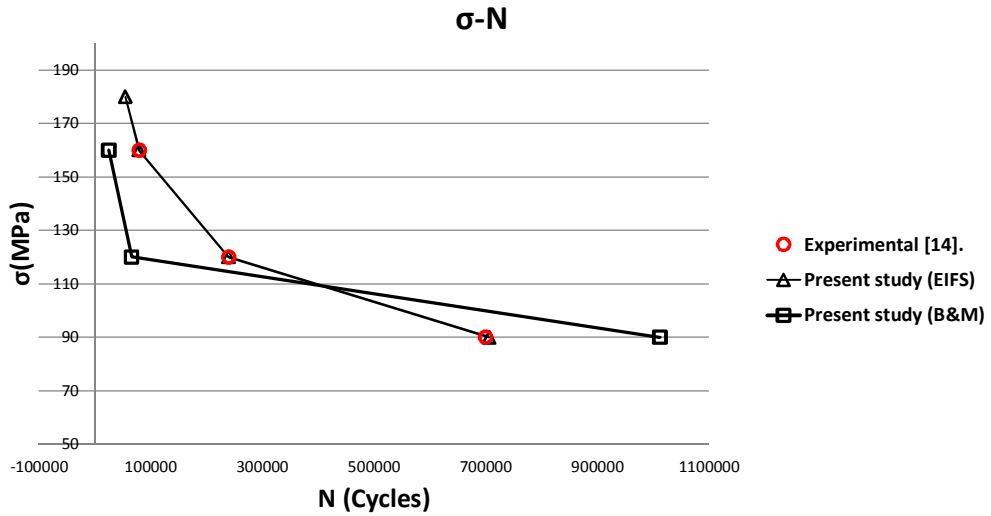

Fig. 22. Comparing life prediction using B&M criterion and EIFS concept with the experimental results.

Table 5. Constants of B&M criterion for aluminum AL2024 [29].

σ_f' (Mpa)	835
b	-0.096
$\in_f'$	0.174
C	-0.644
S	0.5

5. Conclusion

This paper considered the numerical modeling of the fatigue crack growth profiles and the life prediction of a simple riveted lap joint based on fracture mechanics using *EIFS* concept. Life of the riveted lap joint was also predicted based on the conventional method using B&M critical plane criterion. The main conclusions can be summarized as follows:

- Simulation results demonstrated that mode I was dominated on the one side of the plates and the crack straightly grew on this side. In contrast, the other side of the plates was in a mixed-mode condition and the crack propagation path was not straight on this side. Thus, the crack growth profiles were not on the same plane.
- *EIFS* depended on loading amplitude if cyclic stress intensity factor were used in *EIFS* estimation along with back extrapolation method. In contrast, while using *J* integral, *EIFS* dependency on loading amplitude reduced so significantly that can be considered as a constant.
- The predicted life based on the fracture mechanics using *EIFS* concept was in very good agreement with the experimental results, as was expected.
- The estimated life by B&M criterion had no good accuracy as compared to the life predicted by the fracture mechanics approach using *EIFS* concept.

References

[1] G. Keceliogli, "*Stress and Fracture Analysis of Riveted Joints"*, M. S. thesis, Middle East Technical University, Turkey, (2008).

[2] E. N. Dowling, *Mechanical Behavior of Materials*, 2nd ed., Prentice-Hall, New Jersey, (1999).

[3] J. J. Newman, "The merging of fatigue and fracture mechanics concepts", *Progress in Aerospace Sciences*, Vol. 34, No. 5-6, pp. 347–390, (1998).

[4] Y. Liu and S. Mahadevan, "Probabilistic fatigue life prediction using an equivalent initial flaw size distribution", *International Journal of Fatigue*, Vol. 31, No. 3, pp. 476–487, (2009).

[5] J. J. Newman, E. Phillips and M. Swain, "Fatigue-life prediction methodology using small crack theory", *International Journal of Fatigue*, Vol. 21, No. 2, pp. 109–119, (1999).

[6] J. J. Newman, "Crack Closure Model for Predicting Fatigue Crack-Growth under Aircraft Spectrum Loading. American Society of Testing and Materials", *American Society of Testing and Materials*, STP. 748, pp. 53-84, (1981).

[7] F. Polo, *Equivalent Initial Flaw Size on Open Hole INASCO Specimens*, ADMIRE PROJECT, University of Porto, Portugal, (2004).

[8] L. Molent, Q. Sun and A. Green, "Characterization of equivalent initial flaw sizes in 7050 aluminum alloy", *Fatigue and Fracture of Engineering Materials and Structures*, Vol. 29, No. 11, pp. 916-937, (2006).

[9] A. Makeev, Y. Nikishkov and E. Armanios, "A concept for quantifying equivalent initial flaw size distribution in fracture mechanics based life prediction models", *International Journal of Fatigue*, Vol. 29, No. 1, pp. 141-145, (2007).

[10] S. Pitt and R. Jones, "Multiple-site and widespread fatigue damage in aging aircraft", *Engineering Failure Analysis*, Vol. 4, No. 4, pp. 237-257, (1997).

[11] A. Atre, "A Finite Element and Experimental Investigation on the Fatigue of Riveted Lap Joints in Aircraft Applications", *PhD thesis*, Georgia Institute of Technology, USA, (2006).

[12] L. Silva, J. Gonçalves, F. Oliveira and P. Castro, "Multiple Site Damage in Riveted Lap-Joints: Experimental Simulation and Finite Element Prediction", *International Journal of Fatigue*, Vol. 22, No. 4, pp. 319-338, (2000).

[13] R. Piascik, S. Willard and M. Miller, "The characterization of widespread fatigue damage in fuselage", *NASA Technical Memorandum* 109142, USA, (1994).

[14] P. Moreira, P. Matos, P. Camanho, P. Pastrama and P. Castro, "Stress intensity factor and load transfer analysis of a cracked riveted lap joint", *Materials and Design*, Vol. 28, No. 4, pp. 1263-1270, (2007).

[15] A. Skorupa, M. Skorupa, T. Machniewicz and A. Korbel, "Fatigue crack location and fatigue life for riveted lap joints in aircraft fuselage", *International Journal of Fatigue*, Vol. 58, *January*, pp. 209-217, (2014).

[16] J. Park and S. Atluri, "Fatigue Growth of Multi-Cracks Near a Row of Fastener-Holes in a Fuselage Lap-Joint", *Computational Mechanics*, Vol. 13, No. 3, pp.189-203, (1993).

[17] J. Beuth and J. Hutchinson, "Fracture analysis of multi-site cracking in fuselage lap joints", *Computational Mechanics*, Vol. 13, No. 5, pp. 315-331, (1994).

[18] C. Harris, R. Piascik and J. Newman, "A practical engineering approach to predicting fatigue crack growth in riveted lap joints". *Proc. of International Conference on Aeronautical Fatigue"*, W.A. Seattle, (1999).

[19] J. Hou, M. Goldstraw, S. Maan and M. Knop, "An Evaluation of 3D Crack Growth Using ZENCRACK", *DSTO Aeronautical and Maritime Research Laboratory*, Australia, (2001).

[20] T. Hellen, "On the method of virtual crack extensions", *International Journal for Numerical Methods In Engineering*, Vol. 9, No. 1, pp. 187-207, (1975).

[21] R. Billardon, C. Adam and J. Lemaitre, "Study of the non-uniform growth of a plane crack in a three-dimensional body subjected to non-proportional loadings", *International Journal of Solids Structures*, (1986).

[22] ZENCRACK user manual, Issue 7.5, Zentech Inc, (2008).

[23] P. Moreira, P. Matos and P. Castro, "Fatigue striation spacing and equivalent initial flaw size in Al 2024-T3 riveted specimens", *Theoretical and Applied Fracture Mechanics*, Vol. 43, No. 1, pp. 89-99, (2005).

[24] A. Shahani, H. Moayeri Kashani, M. Rastegar and M. Botshekanan Dehkordi, "A unified model for the fatigue crack growth rate in variable stress ratio", *Fatigue and Fracture of Engineering Materials and Structures*, Vol. 32, No. 2, pp.105-118, (2009).

[25] J. Draper, *Modern Metal Fatigue Analysis*, Safe Technology Limited, Sheffield, UK, (2004).

[26] D. Socie and G. Marquis, *Multiaxial Fatigue*, SAE, USA, (2000).

[27] ASTM-E466, "Standard Practice for Conducting force controlled constant amplitude axial fatigue tests of metallic materials", Annual Book of ASTM Standards, (1991).

[28] ASTM-E606, "Standard Practice for Strain-Controlled Fatigue Testing", Annual Book of ASTM Standards, (1998).

[29] C. Boller, and T. Seeger, *Material Data for Cyclic Loading-Part D: Aluminum and Titanium Alloys*, Material Science Monographs 42D, Elsevier, Amsterdam, (1978).